Effective thermal potential between static Q and $\bar{Q}$ in SU(3) gauge theory

Dibyendu Bala[*]

Tata Institute of Fundamental Research
E-mail: dibyendu@theory.tifr.res.in

Saumen Datta

Tata Institute of Fundamental Research
E-mail: saumen@theory.tifr.res.in

A non-perturbative calculation of the effective thermal potential between heavy Q and $\bar{Q}$ from lattice QCD is difficult, and usually involves a Bayesian analysis. Here we present a simple method to obtain the potential from smeared Wilson loop, using the structure of the thermal Wilson loop. We present results for the $Q\bar{Q}$ thermal potential in a gluonic plasma for temperatures $\lesssim 2T_c$. We also present preliminary results for the effective potential when the Q and $\bar{Q}$ are in octet color configuration.

---

[*]Speaker.

1. Introduction

Quarkonium is an important probe of quark-gluon plasma formation in relativistic heavy ion collision experiments. One can define an effective "thermal potential" to understand the medium modification of quarkonia [1]. The thermal potential plays an important role in the treatment of in-medium quarkonia as open quantum system [2]. To define the potential at finite temperature consider the real time $Q\bar{Q}$ operator, $M(r = |\vec{x} - \vec{y}|, t) = \bar{\psi}(\vec{x}, t) U(\vec{x}, \vec{y}; t) \psi(\vec{y}, t)$. In the static limit, the forward correlation function of this operator $c(r, t) = \langle M(r, t) M^\dagger(r, 0) \rangle$ becomes proportional to a rectangular real time Wilson loop $w(r, t)$. The static potential is defined as [1]

$$V(r) \;=\; i \lim_{t \to \infty} \frac{\partial \log \langle w(r, t) \rangle}{\partial t}. \tag{1.1}$$

Eqn. (1.1) has been calculated in leading order HTL perturbation theory. It gives a complex potential: $V(r) = V_T^{\text{re}}(r) - i V_T^{\text{im}}(r)$, with $V_T^{\text{re}}(r)$ the usual Debye-screened Coulomb potential and

$$V_T^{\text{im}}(r) \;=\; \frac{2g^2 T}{3\pi} \int_0^\infty dz \, \frac{z}{(z^2 + 1)^2} \left(1 - \frac{\sin z m_D r}{z m_D r} \right). \tag{1.2}$$

Here T denotes the temperature, and m_D is the Debye mass.

On the lattice we can only calculate Euclidean-time Wilson loop $w_E(r, \tau)$, defined in the time interval $\tau = [0, \beta = 1/T)$. This can be connected to the real-time Wilson loop $w(r, t)$ through a spectral function $\rho(\omega)$ [3],

$$\langle w_E(r, \tau) \rangle = \int_{-\infty}^\infty d\omega \, \rho(\omega) \, e^{-\omega \tau}. \tag{1.3}$$

$w(r, t)$ can be constructed by taking Fourier transform of $\rho(\omega)$. On lattice obtaining $\rho(\omega)$ is very difficult problem as we have only small number of data points along the temporal direction.

There have been attempts to calculate $\rho(\omega)$ using various Bayesian analysis methods. Maximum Entropy method was used in Ref. [3]; however the potential obtained there was not screened above T_c. Also the quality of signal for Wilson loop deteriorates very fast with the size of the loop. To improve the signal, we have used multilevel algorithm, slicing the lattice in τ direction, and used APE smeared spatial links in the construction of the Wilson loop. If a suitable potential can be defined, it should not depend on the smearing of the spatial link; we have checked this by using various levels of smearing. In the literature Coulomb gauge fixed Wilson line correlators have often been used to extract the potential. Bayesian reconstruction of such a correlator has shown a screened potential, and the imaginary part of the potential has also been obtained [4]. However the results have large errors [4]. There are also studies using the method of moments and making some ansatz for the form of $\rho(\omega)$ [5].

We use a different analysis method, using the structure of the Wilson loop; our method will be described in the next section. In Sec. 3 we will show the results for the potential for gluonic plasma. More details regarding these can be found in Ref. [6].

For QGP phenomenology, one needs the thermal potential not only between $Q\bar{Q}$ in the singlet channel, but also when they are in an octet color configuration. The octet potential is also a necessary ingredient for the open quantum system approach [2]. In Sec. 4 we discuss the interaction potential between the static Q and $\bar{Q}$ in a color-octet configuration.

2. Method

At zero temperature $\langle w_E(r,\tau;T=0)\rangle \sim e^{-V(r)\tau}$ at large τ; as a result one would see a plateau in the effective mass $m_{eff}(r,\tau_i) = log\frac{\langle w_E(r,\tau_i)\rangle}{\langle w_E(r,\tau_i+1)\rangle}$. $V(r)$ determined from lattice is qualitatively similar to the Cornell potential. However at finite temperature above T_c there is no plateau in the effective mass. Given that $V_T(r)$ is expected to have an imaginary part [1], one should not expect a plateau either.

Motivated from HTL perturbation theory, we split $w_E(r,\tau)$ as:

$$\log\left(\langle w_E(r,\tau)\rangle\right) = \frac{1}{2}\log\left(\frac{\langle w_E(r,\tau)\rangle}{\langle w_E(r,\beta-\tau)\rangle}\right) + \frac{1}{2}\log\left(\langle w_E(r,\tau)\rangle\langle w_E(r,\beta-\tau)\rangle\right). \tag{2.1}$$

Let us first focus on the anti-periodic part $A(r,\tau) = \frac{1}{2}\log\left(\frac{\langle w_E(r,\tau)\rangle}{\langle w_E(r,\beta-\tau)\rangle}\right)$. From perturbation theory one expects $A(r,\tau) = (\frac{\beta}{2}-\tau)V_T^{\text{re}}(r)$. In the left panel of Fig 1 we have plotted the effective mass $m(r,\tau)$ and $\frac{A(r,\tau)}{(\beta/2-\tau)}$. From the figure it is clear that non-perturbatively also $A(r,\tau)$ is linear in τ around $\beta/2$. For the remaining part, $P(r,\tau) = \frac{1}{2}\log(\langle w_E(r,\tau)\rangle\langle w_E(r,\beta-\tau)\rangle)$, we can again take help from perturbation theory and write it as

$$P(r,\tau) = \int_{-\infty}^{\infty} d\omega\, \sigma(\omega)\left(e^{-\omega\tau} + e^{-\omega(\beta-\tau)} + \tau \text{ independent parts}\right). \tag{2.2}$$

Now to have a potential $i\partial_t P(r,it)$ should approach a constant as t goes to infinity.

$$i\partial_t P(r,it) = \int_{-\infty}^{\infty} (e^{-i\omega t} - e^{-\omega(\beta-it)})\,\omega\,\sigma(\omega)\,d\omega. \tag{2.3}$$

Therefore we need $\sigma(\omega)$ to go like $\sigma(\omega) \sim \frac{1}{\omega^2}$ as ω approaches zero. On the right panel of Fig. 1 we have shown a fit of $\partial_\tau P(r,\tau)$ calculated from lattice data with the leading $\frac{1}{\omega^2}$ behaviour. We can see that almost the entire range of τ can be fitted with this leading singular structure.

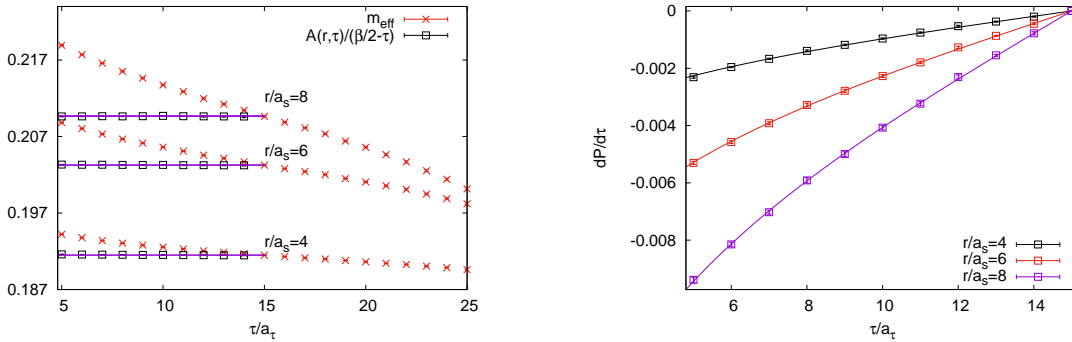**Figure 1:** (Left) Comparison of effective mass for $m(r,\tau)$ and $A(r,\tau)/(\beta/2-\tau)$ for 1.5 T_c. (Right) $\frac{dP(r,\tau)}{d\tau}$; see the discussion around Eq.(2.3).

One of the $1/\omega$ in $1/\omega^2$ comes from a factor $1+n_b(\omega)$, where $n_b(\omega)$ is the Bose distribution function [1]. This can be understood from the structure of the time-ordered correlator [6]. Therefore we expand $\sigma(\omega)$ in the following form,

$$\sigma(\omega) = (1+n_b(\omega))\left(\frac{\beta V_{im}}{2\pi\omega} + c_1\omega + c_2\omega^3 + ...\right). \tag{2.4}$$

Only the odd terms are present because the even ones do not contribute to Eq. (2.2). A very good fit of the data can also be found just by using two terms in the series. The potential is obtained from the coefficient of $1/\omega$ in the expansion, as only this term contributes in the long time t limit. Using Eq. (2.4) one would then get

$$\partial_\tau P(r, \tau) = V_{\text{im}} \cot(\frac{\pi \tau}{\beta}) + c_1 G_1(\tau, \beta) + c_2 G_2(\tau, \beta) + ... \tag{2.5}$$

$$G_n(\tau, \beta) = \frac{2(2n)!}{\beta^{2n+1}} \left(\zeta\left(2n+1, \frac{\tau}{\beta}\right) - \zeta\left(2n+1, 1-\frac{\tau}{\beta}\right) \right).$$

Our strategy for calculating potential is then obvious: we do a linear fit of $A(r, \tau)$ near $\beta/2$ to get the real part of the potential and the imaginary part can be obtained by fitting Eq. (2.5) More details on the analysis can be found in [6].

3. Results for singlet channel

We show here the results of the singlet potential obtained from anisotropic lattices with coupling $\beta = 6.64$ and the bare anisotropy $\xi_b = 2.55$, which corresponds to a renormalized anisotropy $\xi = 3$ and a spatial lattice spacing of 0.048 fm. For results with other lattice parameters and discussion of cutoff effects see [6]. The spatial volume was kept fixed at 1.44 fm, and temperatures upto 2 T_c were explored by varying the temporal extent N_t. We used APE smearing for the spatial links of the Wilson loop. The potential was calculated with various number of smearing steps, where each smearing step involved replacing the spatial links $U_{\vec{x}}^i$ by $\text{Proj}_{SU(3)} \left(\alpha U_{\vec{x}}^i + \sum_{j \neq i} U_{\vec{x}}^j U_{\vec{x}+\hat{j}a}^i U_{\vec{x}+\hat{i}a}^{j\dagger} \right)$, with $\alpha = 2.5$.
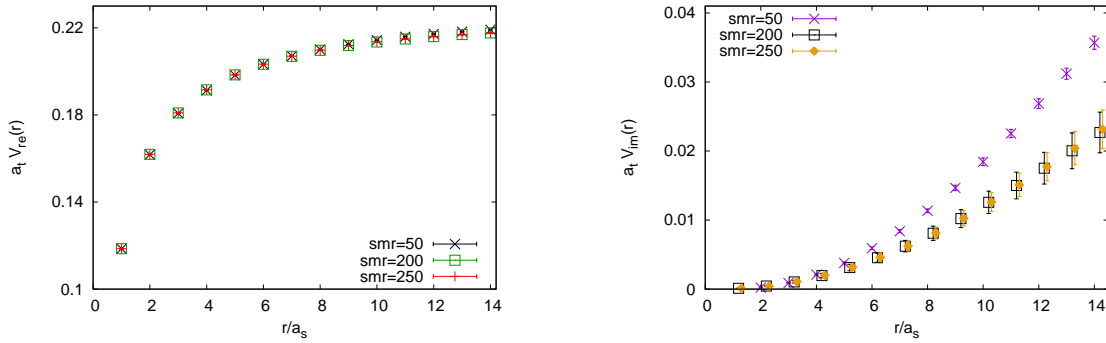

Figure 2: (Left) $V_T^{\text{re}}(r)$ and (right) $V_T^{\text{im}}(r)$ at 1.5 T_c, calculated with different levels of APE smearing.

In Fig. 2 we have plotted the real and imaginary parts of the potential as a function of the number of smearing sweeps for $T = 1.5T_c$. From the figure it is clear that the potential has very minor dependence on the smearing after a certain number of smearing. Anyway for the calculation of error we have included the variation with respect to smearing as a systematic error. When quoting the value of imaginary part the error also includes the variation of the fit results when we change the number of terms in Eq. (2.4).

In Fig. 3 we show the temperature dependence of the singlet potential. $V_T^{\text{re}}(r)$, shown in the left panel, shows a clear screening behavior above T_c. At a temperature of 0.75 T_c $V_T^{\text{re}}(r)$ shows the
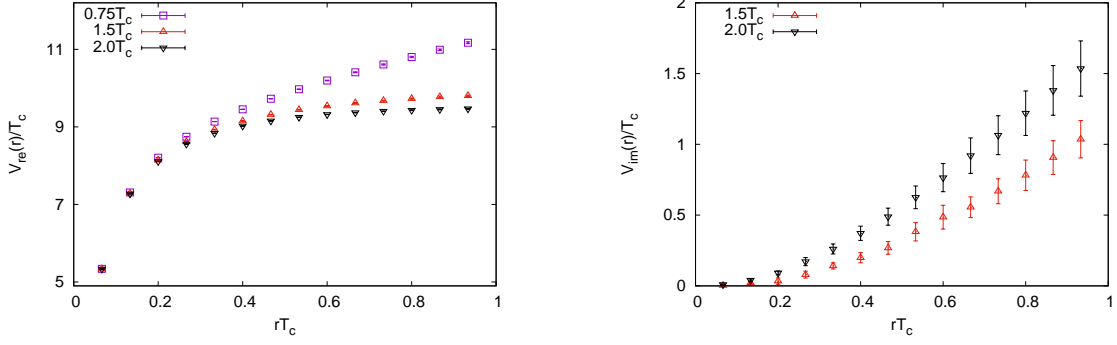
Figure 3: (Left) $V_T^{\mathrm{re}}(r)$ and (right) $V_T^{\mathrm{im}}(r)$ at different temperatures.

usual linear string tension behavior at long distances. Above T_c this linear rise is screened, with the screening increasing with temperature. However, quantitatively the potential is different from the screened Coulomb form; addition of a screened string tension term [7] is needed to fit $V_T^{\mathrm{re}}(r)$ at these temperatures.

On the right hand side we have plotted $V_T^{\mathrm{im}}(r)$. The results below T_c are consistent with zero and are not shown in the plot. Above T_c, $V_T^{\mathrm{im}}(r)$ is very different from the perturbative results of Ref. [1]. It is also seen to increase with rise in temperature. More details about the temperature dependence and parametrization of $V_T^{\mathrm{im}}(r)$ can be found in Ref. [6].

4. Results for octet channel

For phenomenology of quarkonia in QGP, one also needs to understand the interaction between Q and $\bar{Q}$ when they are in a color octet configuration. In analogy with the singlet state, we can try to define a potential using the point-split operator $\bar{\psi}(\vec{x},t)U(\vec{x},\vec{x}_0;t)T_aU(\vec{x}_0,\vec{y};t)\psi(\vec{y},t)$ [8]. This state, however, is not gauge invariant.

A gauge invariant state with the quark content of the above operator can be formed by adding a color-adjoint gluonic operator H_a [9]:

$$\mathscr{O}(r = |\vec{x} - \vec{y}|, t; \vec{x}_0) = \bar{\psi}(\vec{x},t)U(\vec{x},\vec{x}_0;t)T_aH_a(\vec{x}_0,t)U(\vec{x}_0,\vec{y};t)\psi(\vec{y},t). \tag{4.1}$$

Taking the above source will, in the static limit, lead to Wilson loop with inserted $T_aH_a(\vec{x}_0)$ at both initial and final time slices. Here we take two operators, B_a^z and $B_a^x + iB_a^y$, for H_a, where the quark and the antiquark are taken to be separated in the z direction. These are the hybrid states with gluonic angular momentum $L = 0$ and $L = 1$ along z direction for B_a^z and $B_a^x + iB_a^y$ respectively. The results shown in this section are from Wilson loops with 200 steps of smearing for spatial links.

In the left panel of Fig. 4 we show the octet potential at the temperature of 0.75 T_c. For comparison, the singlet potential at this temperature is also shown. As with the singlet channel, below T_c the potential is largely insensitive to temperature and closely resembles the zero temperature potential. In leading order perturbation theory these hybrid potentials at short distances only get contribution from octet channel, and the potential is independent of H_a [9] at short distance. However, at long distance the potential depends on H_a [9], leading to different hybrid potentials for the $L = 0$ and $L = 1$ channels.
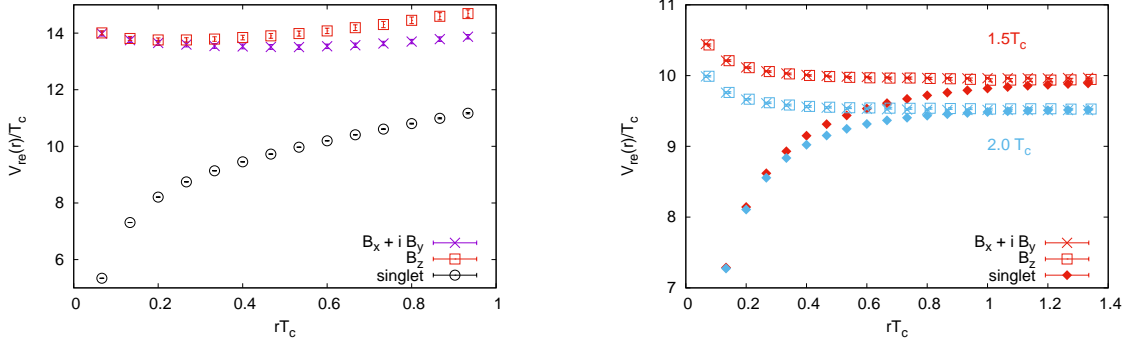
4

Figure 4: Singlet and "octet" potentials between static Q and $\bar{Q}$ below (left, at 0.75 T_c) and above (right) the deconfinement transition temperature.

At finite temperature we have calculated the real part of the potential for the state $\mathcal{O}(r,t)$ using the method of Sec. 2. The plateau structure here is not as good as that of the singlet, however the real part of the potential can be obtained by fitting a few points near $\beta/2$. Preliminary results for the potential are shown in the right panel of Fig. 4. Here we find that the potential is identical for the two choices of H_a we have used. This suggests that at finite temperature the effect of H_a gets decoupled from the potential at all distances, and we can meaningfully talk about the real part of the effective thermal potential for octet $Q\bar{Q}$. Of course, it would be good to further check this with other choices of the gluonic operator.

In the figure we have also shown $V_T^{\mathrm{re}}(r)$ for the singlet potential, at the same temperatures. As the figure shows, the octet and singlet potential approach each other at long distances. At higher temperatures they approach each other at shorter distances. We stress that we did not add any additive renormalization constant to the octet potential to match with singlet: as the effect of H_a gets decoupled, the renormalization of the octet gets fixed once the additive renormalization for the singlet is fixed.

At short distances, the singlet and octet potentials are attractive and repulsive, respectively, consistent with perturbation theory. To further investigate conformity with perturbation theory without having to worry about the additive renormalization constant, we define [10] $\delta V_{o,s}(r) = V_{o,s}(r+a_s) - V_{o,s}(r)$, where o,s stand for octet and singlet, respectively. In leading order of perturbation theory, $\delta V_s(r) = -8\delta V_o(r)$. The nonperturbative estimates, shown in Fig. 5, agree with this prediction within our errorbars.

5. Summary

Extraction of a thermal potential from the Euclidean time Wilson loop is difficult and often involves Bayesian analysis. Here we calculate the complex "thermal potential" [1] using various properties of Wilson loops, motivated from perturbation theory; the method is described in Sec. 2. We have discussed results for the singlet potential in Sec. 3. On crossing T_c, the linear confining part of the real part of the potential is screened, the screening increasing with increase in temperature. However, at least upto temperatures of 2 T_c the singlet $V_T^{\mathrm{re}}(r)$ is different from the perturbative potential. In the deconfined phase, the effective potential also acquires an imaginary
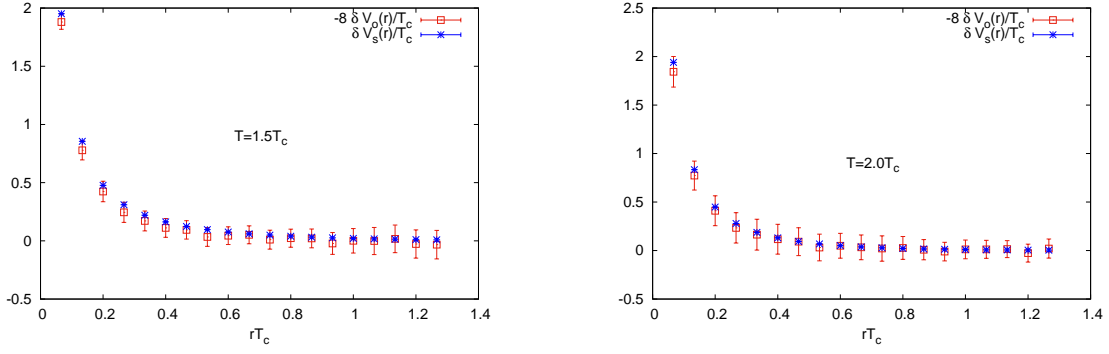
Figure 5: Comparison of octet δV_o and singlet δV_s, at (left) 1.5 T_c and (right) 2.0 T_c. Here for octet, the results for $H_a = B_a^x + iB_a^y$ are shown.

part. The imaginary part is very different from the perurbative result, with the potential not saturating upto the distance scale $rT_c \sim 1.4$, or $r \sim 1$ fm. We have also studied the effective thermal potential between the Q and $\bar{Q}$ in an octet configuration. Preliminary results for the real part of the potential are discussed in Sec. 4. Our results indicate that, unlike at zero temperature, the thermal potential between hybrid states is not sensitive to the gluonic structure in $\mathscr{O}(r)$, Eq. (4.1). While at short distances the octet potential is repulsive, at long distances it approaches the singlet potential. Qualitatively the potential is similar to the free energy for the octet state [11].

References

[1] M. Laine, O. Philipsen, P. Romatschke & M. Tassler, JHEP 0703 (2007) 054.

[2] Y. Akamatsu, Phys. Rev. D 87 (2013) 045016; Phys. Rev. D 91 (2015) 056002.

[3] A. Rothkopf, T. Hatsuda & S Sasaki, Phys. Rev. Lett. 108 (2012) 162001.

[4] Y. Burnier, O. Kaczmarek & Alexander Rothkopf, Phys. Rev. Lett. 114 (2015) 082001 (2015).

[5] P. Petreczky & J. weber, Nuclear Physics A 967 (2017) 592.

[6] D. Bala & S. Datta, arXiv:1909.10548 [hep-lat].

[7] Y. Burnier & A. Rothkopf, Phys. Lett. B 753 (2016) 232

[8] A Bazavov & P Petreczky 2013 J. Phys: Conf. Ser. 432, 012003.

[9] G.S. Bali & A. Pineda, Phys. Rev. D 69 (2004) 094001.

[10] O. Philipsen, Phys. Lett. B 535 (2002) 138.

[11] F. Zantow, O. Kaczmarek, F. Karsch & P. Petreczky, *Proceedings, 5th International Conference on Strong and Electroweak Matter*, World scientific, 2003 (hep-lat/0301015).